IEEE Access
Multidisciplinary | Rapid Review | Open Access Journal

Date of publication xxxx 00, 0000, date of current version xxxx 00, 0000.

Digital Object Identifier 10.1109/ACCESS.2023.0322000

Implicit Euler Discretization for Enhanced Sliding Mode Observer in Sensorless permanent magnet synchronous motor Control

Nehal Baiomy [1], Mohamed M. Abdelhafiz [1], and Abdelmomen Mahgoub[1], (Member, IEEE)
[1]Electrical Power Engineering Department, Cairo University, Giza, 12613 Egypt
Corresponding author: Abdelmomen Mahgoub (e-mail: abdelmomen.mahgoub@cu.edu.eg).

ABSTRACT This paper presents a discrete-time sliding mode observer designed to estimate the rotor position of PMSMs for sensorless control strategies. Without compromising the sliding feature, this study employs a discretization method known as implicit Euler discretization, converting the set-valued function to a projection over a limited interval, simplifying the coding compared to other ordinary implementations. As a result, output chatter is significantly reduced without additional filters. The observer's performance is evaluated under sudden changes in load and parameter variations and then compared with other approaches. The proposed SMO is also tested and validated on an experimental setup of a 600W PMSM coupled with a DC generator for loading. The results show the robustness of the proposed observer, with a reduction in execution time by approximately 20% compared to conventional implementations like the sigmoid-based sliding mode observer.

INDEX TERMS Permanent magnet synchronous motor (PMSM), sensorless control, sliding mode observer (SMO), sigmoid function, implicit Euler discretization.

I. INTRODUCTION

PERMANENT Magnet Synchronous Motors (PMSMs) have become increasingly prevalent in various industrial applications due to their high efficiency, compact size, and excellent torque-to-weight ratio. They are widely utilized in areas such as robotics, automotive industries, aerospace, and renewable energy systems. An essential aspect of PMSM drive systems is the requirement for precise control over rotor position and speed, which has traditionally been achieved through the use of physical sensors [1] to provide feedback within the control framework. However, factors such as cost, size, and robustness of physical sensors necessitate sensorless control approaches for drive systems [2]–[5]. The primary challenge in sensorless PMSM control is achieving accurate and robust estimation of rotor position and speed across various operating conditions, including low-speed and standstill operation. Traditional sensorless methods often struggle with performance issues at low speeds due to weak back-EMF signals, which are essential for position estimation [6], [7]. Furthermore, the dynamic response of sensorless drives is critical, particularly in applications requiring fast and precise control.

Another significant challenge is that motor parameters may change according to the surrounding temperature, increasing the design complexity and computational demands of sensorless control algorithms. Advanced estimation techniques, such as observer-based methods, can provide improved performance, especially when the observation approach is robust enough to handle parameter fluctuations over a wide range of operating speeds [8]. Several observation techniques have been proposed [6], [7], with most using the Luenberger Observer [9], [10]. This observer type has a typical structure as the motor model, plus a feedback term that works on reducing the observation error via a gain vector. However, it may not be able to handle system nonlinearities during operation.

Recently developed observer methods such as the Extended Kalman Filter (EKF) are popular for their ability to estimate system states in nonlinear environments effectively [11]. Bendjedia and Chouireb in [12] employed EKF to achieve optimal performance and stability of the control system for electric vehicles during speed sensor failure or absence. This approach involves developing robust estimation techniques to accurately assess the vehicle's speed using alternative inputs. However, EKF has certain disadvantages. One issue with the EKF is that it can suffer from DC offset, resulting in steady-state errors. It also suffers from non-global con-

vergence, causing its performance to vary greatly depending on the initial conditions. Due to its heavy matrix operations and nonlinear calculations, the EKF also requires significant computational power, especially for real-time applications.

Sliding mode observers (SMOs) have emerged as a robust solution for sensorless control in motor drives. Their ability to maintain performance under system uncertainties and parameter variations distinguishes them from traditional estimation methods. SMOs create a sliding motion on the error between the available measured output of the real system and the estimated output of the observer. Once the sliding mode occurs, the observer ensures that the estimated state precisely follows the actual output of the system [13]. Different techniques based on the sliding mode approach have been proposed [2], [14] to integrate SMOs with advanced control techniques, like vector control and direct torque control, enhancing the performance of sensorless drives. This integration allowed for better handling of dynamic changes and improved overall efficiency.

The conventional sliding mode approach depends on a discontinuity function that gives rise to a coupling problem known as chattering phenomena [15]–[17]. The use of a low-pass filter (LPF) for such phenomena can, however, lead to buffering, reducing the accuracy of the estimated states. One solution to relax the sharp-switched function and thereby lessen the chattering issue is applying a sigmoid function with variable boundary layers in place of a discontinuity characteristic. There is however concern that a steeper sigmoid function would lead to more chattering, so it is crucial to modify the boundary layer width in order to prevent chattering or steady-state errors [3]. For example, Kim *et al.* [18] recommended using heuristic methods to adjust those gains of sigmoid function, while Sheng *et al.* [19] developed a fuzzy technique to adjust same issues. Additionally, the sigmoid function has lengthy computation time due to its exponential behavior, creating a barrier for real-time applications.

Another way to reduce chattering is by using adaptive sliding mode techniques [20]. These methods adjust the sliding mode parameters in real-time based on how the system is performing, which helps to smooth out the control action. Additionally, higher-order sliding mode techniques [21], [22] improve on this by using more advanced derivatives of the sliding surface, not just the first-order ones. This helps to reduce steep changes and makes the control smoother. However, these solutions can be quite complex and less suitable for low-cost real-time applications. Efforts to simplify the mathematical models used in SMOs without compromising performance have been a key focus area. Simplification aims to make these observers more accessible for practical implementation and reduce the expertise required for their deployment.

More than decade ago, Acary and Brogliato [23], [24] presented implicit Euler discretization as a discretization technique to safely suppress chattering without need for extra filters, while preserving the discontinuity feature of sliding surfaces' dynamics. Generally, high sampling rates are not conducive to reducing chattering in discrete sliding mode systems. Contrary to this, implicit Euler discretization allows sampling rates to be freely increased, which typically results in better performance for discrete systems [24]. Among the numerous benefits highlighted here and in more detail in [23]–[25], the feature that stands out to us is the ability to harness the robust characteristics of sliding mode systems without the chattering effect, coupled with straightforward coding implementation. This is particularly advantageous for real-time applications that necessitate an economical controller. The coding simplicity stems from the fact that the output of the discontinues function at each step is reduced to a projection onto the interval $[-1, 1]$. Such a process is relatively simple to encode. This developed technique reflects a trend towards more robust and efficient application, such as sensorless control methods for motor drives. The ongoing research in this field continues to push the boundaries of what is possible with sensorless motor control technologies [4], [19].

Implicit Euler discretization has been tested primarily with control approaches based on sliding mode. Until recently, there have been very limited studies that expand the concept of implicit Euler discretization to an observer approach [26], and to the best of the author's knowledge, it has not been applied to PMSM in particular. The development of a novel SMO, particularly those that simplify design and reduce computational requirements while maintaining accuracy and robustness, is of great interest in the field of controlling sensorless SPMSM. In this context, this paper introduces a sliding mode observer for sensorless PMSM drives adopting the implicit Euler discretization. The proposed sliding mode observer aims to estimate the machine's speed and position based solely on current measurements. The performance of the proposed observer is evaluated by comparing it to other traditional observer structures. The comparison was carried out in both simulated and experimental settings. The objectives of this paper can be summarized as follows;

- Propose a novel discrete-time sliding mode observer based on implicit Euler discretization.
- Validate the use of implicit discretization techniques for sliding mode observers, particularly for practical applications like observing the back EMF of PMSM.
- Analyze the stability of the novel SMO.
- Evaluate the performance of the proposed SMO against low-speed operation, parameter uncertainties, and various load conditions.
- Evaluate the execution time needed to implement the novel SMO compared to other existing observers.
- Validate our findings experimentally.

In this paper, Section II introduces the mathematical model of the PMSM, while Section III discusses the proposed SMO and its implementation in the discrete-time. In Section IV, simulations results and experimental results show the performance of the proposed observer and its validation against sudden changing in load and parameters variations. Finally,

Section VI concludes the significant results of this work.

II. PROBLEM FORMLATION

A. MATHEMATICAL MODEL OF PMSM

In this article, we focus on a type of PMSM known as the surface-mounted (SPMSM) or 'non-salient PMSM', where magnets are mounted directly on the surface of the rotor. This design refines the air gap between the machine parts, resulting in equal inductance along the direct and quadrature axes. Based on the following parameters' definitions;

ω_e	Electrical speed
ω_m	Rotor mechanical speed
θ_m	Rotor angular position
θ_e	Rotor electrical position
i_α, i_β	Stator currents in stationary reference frame (α, β)
v_α, v_β	Stator voltages in stationary reference frame $(\alpha\beta)$
ψ_f	the magnetic flux of the permanent magnet
R_s	Stator resistance
L_s	Stator inductance,

the PMSM model in the stationary reference frame $(\alpha - \beta)$ is modeled as follows:

$$\dot{\mathbf{I}}_{\alpha\beta} = \mathbf{A}\mathbf{I}_{\alpha\beta} + \mathbf{B}(\mathbf{V}_{\alpha\beta} - \mathbf{E}_{\alpha\beta}) \tag{1}$$

in which $\mathbf{I}_{\alpha\beta} = [i_\alpha \quad i_\beta]^T$, $\mathbf{V} = [v_\alpha \quad v_\beta]^T$,

$$\mathbf{A} = \begin{bmatrix} -\frac{R_s}{L_s} & 0 \\ 0 & -\frac{R_s}{L_s} \end{bmatrix}, \mathbf{B} = \begin{bmatrix} \frac{1}{L_s} & 0 \\ 0 & \frac{1}{L_s} \end{bmatrix}, \tag{2}$$

and $\mathbf{E}_{\alpha\beta}$ is the vector of electromotive forces (EMF), which is defined as follows:

$$\mathbf{E}_{\alpha\beta} := \begin{bmatrix} e_\alpha \\ e_\beta \end{bmatrix} = \begin{bmatrix} -\psi_f \omega_e \sin\theta_e \\ \psi_f \omega_e \cos\theta_e \end{bmatrix}. \tag{3}$$

As the motor operates, the back-EMF is generated and fundamentally linked to the speed and position of the rotor as depicted in (3). In field-oriented control (FOC), the position θ_e is essential to complete the overall control loop as shown in Figure 1. Throughout this paper, we aim to obtain an accurate estimation of the back-EMF, which is crucial for sensorless control strategies that eliminate the need for direct rotor position measurement, thus reducing costs and improving the system's robustness.

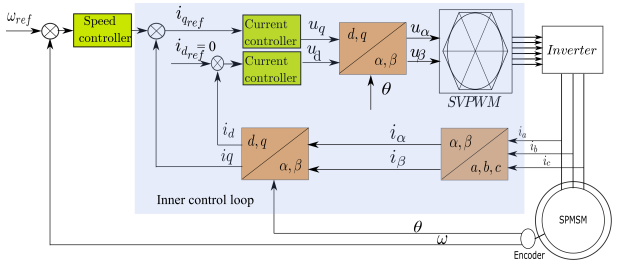

FIGURE 1. Block diagram of field oriented control (FOC) of SPMSM

III. PROPOSED SLIDING-MODE CURRENT OBSERVER FOR BACK-EMF ESTIMATION

A sliding mode observer is a type of nonlinear observer that utilizes the concept of sliding mode control to achieve robust performance under uncertain or disturbing conditions. The conventional implementation of the sliding mode technique can cause chattering and high-frequency oscillations in the produced signal [15], [16]. Various techniques, such as boundary layer smoothing, higher-order sliding modes, and continuous approximations of the switching function, are available to mitigate these issues. However, while these methods aim to minimize or eliminate the chattering effect, they often fail to retain the robustness features of the actual sliding mode approach.

This section adopts a discretization method called 'implicit Euler discretization', which is a promising method introduced by Acary *et al.* [24] to suppress numerical chattering. In addition, implicit Euler discretization has the following core advantages [23], [24]; first, it preserves the sliding surface of the continuous-time system (the discretization does not modify the sliding surface); second, a finite sampling frequency guarantees sliding motion for the discrete-time system. This enhances the practical applicability of SMO in real-world motor control systems.

To successfully observe the BEMF, we first need to check the observability property, which is a mandatory test to determine whether the desired motor states can be accurately estimated regardless of the observation technique used. In the manner of nonlinear observability [27], many studies [17], [28], [29] discuss the observability of non-salient PMSM, where

$$\omega_m \neq 0 \tag{4}$$

is the only condition for the observability of SPMSM. Considering this condition as a prerequisite in this paper, we propose an implicit Euler discretization-based SMO for PMSM.

A. SMO CONSTRUCTION IN CONTINUOUS-TIME

The objective here is to construct a basic sliding mode observer that can resemble the current dynamic in the α-β frame. First, we should select a pre-determined surface (called a sliding surface), on which the system moves along, and is maintained by a switching function in response to disturbances or uncertainty. Based on that, we introduce the following sliding surface;

$$\mathbf{\Sigma}_{\alpha\beta} = \begin{bmatrix} \sigma_\alpha \\ \sigma_\beta \end{bmatrix} = \begin{bmatrix} \hat{i}_\alpha - i_\alpha \\ \hat{i}_\beta - i_\beta \end{bmatrix} \tag{5}$$

From now on, the following switching functions will be used extensively:

$$\mathrm{sgn}(x) \triangleq \begin{cases} [-1, 1] & \text{if } x = 0 \\ x/|x| & \text{if } x \neq 0, \end{cases} \tag{6}$$

$$\mathrm{sat}_\alpha(x) \triangleq \begin{cases} x & \text{if } |x| \leq \alpha \\ \alpha x/|x| & \text{if } |x| > \alpha. \end{cases} \tag{7}$$

Now we can write the sliding mode-based current observer as follows:

$$\dot{\hat{\mathbf{I}}}_{\alpha\beta} \in \mathbf{A}\hat{\mathbf{I}}_{\alpha\beta} + \mathbf{B}(\ \mathbf{V}_{\alpha\beta} - \eta \mathrm{sgn}(\mathbf{\Sigma}_{\alpha\beta})) \tag{8}$$

where

$$\mathrm{sgn}(\mathbf{\Sigma}_{\alpha\beta}) = \begin{bmatrix} \mathrm{sgn}(\sigma_\alpha) \\ \mathrm{sgn}(\sigma_\beta) \end{bmatrix}, \tag{9}$$

and η is a positive scalar selected based on stability analysis as shown later in this section.

B. SLIDING MODE REACHABILITY CONDITION

It is worth noting that the above representation (8) of the current observer considers the back EMF as a matched disturbance that is attenuated by the discontinuous action $\eta \mathrm{sgn}(\mathbf{\Sigma}_{\alpha\beta})$ to keep the estimated current state follows the measured one. This representation is also adopted in [19], in which the error dynamics is written as follows:

$$\dot{\mathbf{\Sigma}}_{\alpha\beta} \in \mathbf{A}\mathbf{\Sigma}_{\alpha\beta} + \mathbf{B}[\mathbf{E}_{\alpha\beta} - \eta \mathrm{sgn}(\mathbf{\Sigma}_{\alpha\beta})]. \tag{10}$$

To analyze the behavior of the error equation (10), which reflects the sliding motion behavior, we introduce the following lyapunov function;

$$V(\mathbf{\Sigma}_{\alpha\beta}) = \frac{1}{2}\mathbf{\Sigma}_{\alpha\beta}^T \mathbf{\Sigma}_{\alpha\beta}, \tag{11}$$

where $V(\mathbf{\Sigma}_{\alpha\beta})$ is a positive definite function for all $\mathbf{\Sigma}_{\alpha\beta} \neq \mathbf{0}$. To ensure that the system's state reaches the sliding surface $\mathbf{\Sigma}_{\alpha\beta} = \mathbf{0}$, we examine the time derivative of $V(\mathbf{\Sigma}_{\alpha\beta})$ as follows;

$$\begin{aligned} \dot{V} &= \dot{\mathbf{\Sigma}}_{\alpha\beta}^T \mathbf{\Sigma}_{\alpha\beta} \\ &= \mathbf{\Sigma}_{\alpha\beta}^T \mathbf{A}^T \mathbf{\Sigma}_{\alpha\beta} + [\mathbf{E}_{\alpha\beta}^T - \eta \mathrm{sgn}(\mathbf{\Sigma}_{\alpha\beta}^T)\mathbf{B}^T \mathbf{\Sigma}_{\alpha\beta} \end{aligned} \tag{12}$$

in which $\mathbf{A}$ is a negative definite matrix, and one can see that

$$\eta > \|\mathbf{E}_{\alpha\beta}\|_\infty \tag{13}$$

is the only sufficient condition to keep the negative definiteness of $\dot{V}$. Consequently, the system's state converges and holds on the sliding surface $\mathbf{\Sigma}_{\alpha\beta} = \mathbf{0}$ as long as condition (13) is true.

C. SMO IMPLEMENTATION IN DISCRETE-TIME

Before introducing the implicit-based discrete-time implementation of the basic SMO, we will briefly discuss how the implicit technique overcomes the chattering problem. Let us consider the following benchmark problem; $\dot{x}(t) \in -a\mathrm{sgn}(x(t))$, where $a > 0$. The traditional discretization reveals that $(x(k+1) - x(k)) \in -aT\mathrm{sgn}(x(k))$ where k is the interval index and T is the sampling time interval. The source of chattering comes when $x(k)$ lies in the discontinuous interval $[-aT, aT]$, for example, in the positive interval $0 < x(k) < aT$, one can see that $x(k+1) \in x(k) - aTsgn(x(k)) < 0$, which indicates continuous changing in the sign of state x at each sampling interval as long as $|x(k)| < aT$. Meanwhile, the implicit discretization suggests considering the input of the discontinuous function to be the predicted solution as follows; $x(k+1) \in x(k) - aTsgn(x(k+1))$. As a result of this configuration, the value of $\mathrm{sgn}(x(k+1))$ can be selected to be equal to $x(k)/aT$, which is a projection inside $[-1, 1]$, so that $x(k+1)$ is pushed to zero, and thus the chattering phenomenon is eliminated. Roughly speaking, the implicit technique considers the interaction between the input to the set-valued function sgn and the system state as an algebraic constraint. This technique uses the nominal model of the controlled plant as a predictor of the system state, which is done by giving a precise value for the set-valued function sgn. Kikuuwe *et al.* [30] map this algebric constrain and propose its solution simply in the following relation;

$$Y \in a\mathrm{sgn}(z - Y) \Longleftrightarrow Y = \mathrm{sat}_a(z), \quad \forall y \in R, \forall z \in R. \tag{14}$$

This again demonstrates the implicit technique's effectiveness in preventing chattering when the saturation function is introduced into the solution. Further analysis for implicit technique performance and its stability is excessively proposed in [24], [31].

Now let us back to the continuous-time system (1) and introduce its discrete-time version as follows:

$$\mathbf{I}_{\alpha\beta(k+1)} = \mathbf{A_d}\mathbf{I}_{\alpha\beta(k)} + \mathbf{B_d}\mathbf{V}_{\alpha\beta_{(k)}} - \mathbf{B_d}\mathbf{E}_{\alpha\beta_{(k)}}, \tag{15}$$

where $\mathbf{A_d} = \mathrm{e}^{\mathbf{A}T} \simeq I + \mathbf{A}T$, $\mathbf{B_d} = \int_0^T \mathrm{e}^{\mathbf{A}\tau} d\tau . \mathbf{B} \simeq T\mathbf{B}$ and T is the sample-time interval. Here we introduce the discrete-time version of the observer (8) based on implicit backward-Euler-discretization as follows;

$$\hat{\mathbf{I}}_{\alpha\beta(k+1)} \in \mathbf{A_d}\hat{\mathbf{I}}_{\alpha\beta(k)} + \mathbf{B_d}\mathbf{V}_{\alpha\beta_{(k)}} - \mathbf{B_d}\eta \mathrm{sgn}(\mathbf{\Sigma}_{\alpha\beta})_{(k+1)}, \tag{16}$$

in which we define the discontinuous action at time index $(k+1)$ as;

$$\mathrm{sgn}(\mathbf{\Sigma}_{\alpha\beta})_{(k+1)} \triangleq \mathrm{sgn}(\hat{\mathbf{I}}_{\alpha\beta(k+1)} - \tilde{\mathbf{I}}_{\alpha\beta(k+1)}). \tag{17}$$

where

$$\tilde{\mathbf{I}}_{\alpha\beta(k+1)} := \mathbf{A_d}\mathbf{I}_{\alpha\beta(k)} + \mathbf{B_d}\mathbf{V}_{\alpha\beta_{(k)}}. \tag{18}$$

The observer state vector $\hat{\mathbf{I}}_{\alpha\beta(k+1)}$ in (16) implicitly appears now inside the discontinuous action, or in other words, the instant observed state vector in (16) feeds the set-valued function sgn in a closed loop. This implementation reflects the approach of the implicit technique, then to solve (16), let us first rewrite it as follows;

$$\begin{aligned} \hat{\mathbf{I}}_{\alpha\beta(k+1)} &- \mathbf{A_d}\hat{\mathbf{I}}_{\alpha\beta(k)} - \mathbf{B_d}\mathbf{V}_{\alpha\beta_{(k)}} \\ &\in \mathbf{B_d}\eta \mathrm{sgn}\Big([\tilde{\mathbf{I}}_{\alpha\beta(k+1)} - \mathbf{A_d}\hat{\mathbf{I}}_{\alpha\beta(k)} - \mathbf{B_d}\mathbf{V}_{\alpha\beta_{(k)}}] \\ &\qquad - [\hat{\mathbf{I}}_{\alpha\beta(k+1)} - \mathbf{A_d}\hat{\mathbf{I}}_{\alpha\beta(k)} - \mathbf{B_d}\mathbf{V}_{\alpha\beta_{(k)}}]\Big), \end{aligned} \tag{19}$$

and thanks to relation (14), we can now handle (19) so that the estimated state vector at $(k+1)$ only appears in the left-hand side as in the following construction:

$$\hat{\mathbf{I}}_{\alpha\beta(k+1)} = \mathbf{A_d}\hat{\mathbf{I}}_{\alpha\beta(k)} + \mathbf{B_d}\mathbf{V}_{\alpha\beta(k)} + \mathrm{sat}_{\eta\mathbf{B_d}}(\tilde{\mathbf{I}}_{\alpha\beta(k+1)} - \mathbf{A_d}\hat{\mathbf{I}}_{\alpha\beta(k)} - \mathbf{B_d}\mathbf{V}_{\alpha\beta(k)}) \quad (20)$$

and by substituting in (20) by (18) , the final configuration of the proposed observer is

$$\hat{\mathbf{I}}_{\alpha\beta(k+1)} = \mathbf{A_d}\hat{\mathbf{I}}_{\alpha\beta(k)} + \mathbf{B_d}\mathbf{V}_{\alpha\beta(k)} + \mathrm{sat}_{\eta\mathbf{B_d}}(\mathbf{A_d}\mathbf{I}_{\alpha\beta(k)} - \mathbf{A_d}\hat{\mathbf{I}}_{\alpha\beta(k)}). \quad (21)$$

Now, one can see that the set-valued function in (19) is indirectly replaced by sat-function, which is a continues function resulting in no numerical chattering in the observed states. Figure 2 shows the implementation of the implicit SMO and its equivalent after utilizing relation (14).

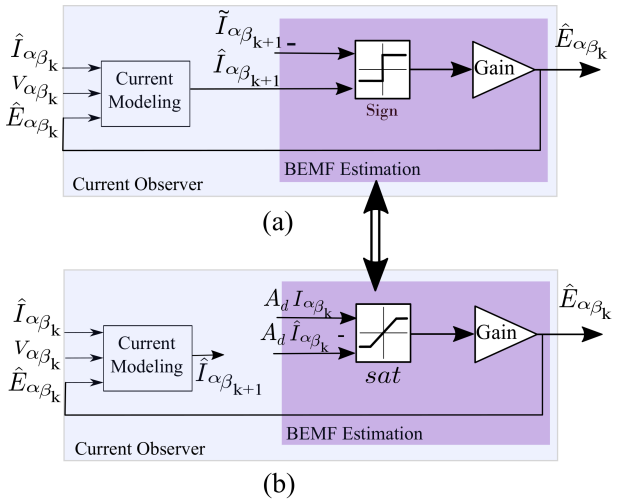

FIGURE 2. The implicit SMO including signum function appears in (a), and its equivalent in (b).

By subtracting (15) from (21), we can see the error dynamics in the discrete-time as follows;

$$\mathbf{\Sigma}_{\alpha\beta(k+1)} = \mathbf{A_d}\mathbf{\Sigma}_{\alpha\beta(k)} + \mathbf{B_d}\mathbf{E}_{\alpha\beta(k)} + \mathrm{sat}_{\eta\mathbf{B_d}}(\mathbf{A_d}\mathbf{I}_{\alpha\beta(k)} - \mathbf{A_d}\hat{I}_{\alpha\beta(k)}) \quad (22)$$

Considering the error dynamic behavior in (22), let us study the stability of the proposed observer in the discrete-time by introducing the following proposition;

Proposition 1. *A Special case of proposition* 1 *in [24]. Considering* $\mathbf{\Sigma}_{\alpha\beta 0}$ *is an initial state for the following discrete-time sliding system;*

$$\begin{cases} \tilde{\mathbf{\Sigma}}_{\alpha\beta(k+1)} = \mathbf{A_d}\mathbf{\Sigma}_{\alpha\beta(k)} - \mathbf{B_d}\eta\mathbf{u}_{(k+1)} \\ \mathbf{u}_{(k+1)} \in \mathrm{sgn}(\tilde{\mathbf{\Sigma}}_{\alpha\beta(k+1)}) \\ \mathbf{\Sigma}_{\alpha\beta(k+1)} = \mathbf{A_d}\mathbf{\Sigma}_{\alpha\beta(k)} + \mathbf{B_d}\mathbf{E}_{\alpha\beta(k)} - \mathbf{B_d}\eta\mathbf{u}_{(k+1)} \end{cases} \quad (23)$$

where its solution is typically (22). Then after a finite number of time-interval k_0, $\tilde{\mathbf{\Sigma}}_{\alpha\beta(k)} = 0$ *and the disturbance* $\mathbf{E}_{\alpha\beta}$ *is attenuated by a factor of the time-interval* T*(* $\Sigma_{\alpha\beta(k)} \propto T\mathbf{E}_{\alpha\beta(k)}$*).*

Proof. See [24, Proposition 1] □

Considering this proposition, one can see that $\mathbf{\Sigma}_{\alpha\beta(k)}$, which is proportional to $T\mathbf{E}_{\alpha\beta(k)}$, approaches zero as $T \searrow 0$, and as a consequence, the switching term in (22) is used to predict $\mathbf{E}_{\alpha\beta(k)}$ as follows;

$$\hat{\mathbf{E}}_{\alpha\beta(k)} = \mathrm{sat}_{\eta\mathbf{B_d}}(\mathbf{A_d}\mathbf{I}_{\alpha\beta(k)} - \mathbf{A_d}\hat{\mathbf{I}}_{\alpha\beta(k)}) \quad (24)$$

Now, based on relation (3), we can finally estimate the electrical position of PMSM as;

$$\hat{\theta}_e = -\arctan(\frac{\hat{e}_\alpha}{\hat{e}_\beta}) \quad (25)$$

Remark 1. *An attractive feature of the implicit Euler method is that it preserves the characteristics of continuous-time systems. To show that, let us consider the behavior of (21) when the sampling interval approaches zero. In this scenario, the following relation between the* sgn *and* sat *functions holds true, as illustrated below:*

$$\lim_{T\searrow 0} \mathrm{sat}_T(x) = \lim_{T\searrow 0} \frac{Tx}{\max(T, |x|)} = T\frac{x}{|x|} = T\mathrm{sgn}(x). \quad (26)$$

Based on this relation, the discrete-time observer in (21) is reduced to

$$\frac{\hat{\mathbf{I}}_{\alpha\beta(k+1)} - \hat{\mathbf{I}}_{\alpha\beta(k)}}{T} \in \mathbf{A}\hat{\mathbf{I}}_{\alpha\beta(k)} + \mathbf{B}\mathbf{V}_{\alpha\beta(k)} - \mathbf{B}\eta\mathrm{sgn}(\hat{\mathbf{I}}_{\alpha\beta(k)} - \mathbf{I}_{\alpha\beta(k)}) \quad (27)$$

which yields the same ordinary discrete version of the continuous-time SMO in (8).

IV. PERFORMANCE EVALUATION

In this section, we will show the performance of the proposed observer against the following conditions: low-speed operation, parameter uncertainties, and various load conditions. The observer loop shown in figure 3 integrated with the main control loop in figure 1 and has been implemented via MATLAB Simulink software. Table 1 shows the parameters of PMSM. A Proportional-Integral (PI) controller is used within the current control loop, and also within the outer control loop of motor speed. The current controller parameters are set as $k_p = 5.278, k_i = 92.857$ and the speed controller parameters are set as $k_p = 0.02244, k_i = 3.77$. These parameters were obtained based on the method outlined in [32]. The test was done under 5 μsec dead-time and $10kHz$ switching frequency. The control method is based on maximum torque per ampere ($i_d = 0$). For the observation loop, the switching gain of the sliding surface is selected as $\eta = 90$, according to (13).

As the back EMF is indirectly derived from the stator voltages and currents, then the estimated back EMF still carries further harmonics as a result of unmodeled dynamics. To enhance the reliability of the estimated position and speed, we applied a second-order low-pass filter (LPF) in a stage before driving the motor angle as in (25). To compensate for

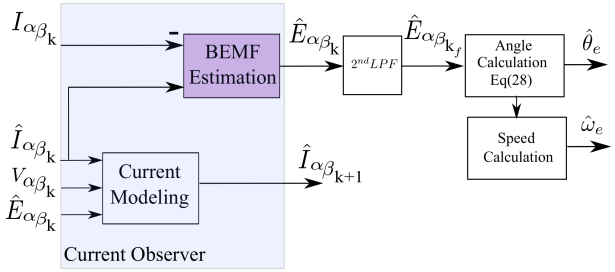

FIGURE 3. Observer loop for Sensorless PMSM

TABLE 1. SPMSM Paramters and Values

Parameter	Value	Parameter	Value
Rated Speed	1000 rpm	Stator Inductance	14 mH
Pole Pairs	5	Stator Resistance	1.3Ω
Flux Linkage	0.112 Wb	Rated Power	600 W
Viscous Friction	0.00193 N.s/m^2	Rated Torque	5.7 N.m
Rotational Inertia	0.0015 kg.m	Dead Time	5 μs
Switching Frequency	10 kHz		

unwanted phase lag due to the LPF, a feed-forward compensation is applied as appears in the following equation;

$$\hat{\theta}_e = -\arctan(\frac{\hat{e}_\alpha}{\hat{e}_\beta}) + \arctan(\frac{\hat{\omega}_e}{\omega_c}) * 2 \qquad (28)$$

where ω_c is the cutoff frequency of the 2^{nd} order filter, and $\hat{\omega}_e$ is the estimated speed obtained as a first derivative of the estimated position.

However the observability condition is only guaranteed when the mechanical speed is not equal to zero, at low speeds, we often have difficulty measuring the BEMF, which is proportional to the estimated rotor position. At such low speeds, noise and unmodeled nonlinearities on the measuring current and voltage are significantly bigger than the fluctuated BEMF. For the same reasons, estimating the initial rotor position is also a challenge that requires following a specific starting method when dealing with observers. Here, we followed the I-f start-up method [33], [34] in an open loop manner by applying $i_q = 0.8\, i_{rated}$, and a ramping speed from 10% up to 20% of the rated speed. Once the error between the reference angle and the estimated one approaches 0.1 *rad*, the sensorless loop is applied.

To evaluate the performance of the proposed observer, four main tests are carried out: the steady-state test, the sudden load change test, the minimum speed test, and the parameter variation test, which we will discuss in the next subsections. We compared the performance of the proposed observer with other two different observer schemes: the conventional Luenberger observer [10], and the sigmoid-based SMO, as shown in figure 4. The sigmoid function is defined as:

$$sigmoid(x) = \frac{2}{1+\exp(-\lambda x)} - 1. \qquad (29)$$

The parameter λ here is a positive-real tunable value. A larger value of λ indicates a rapid rate of boundary layer change, and accordingly, the sigmoid function shape approaches that of the ideal switching function (signum-function).

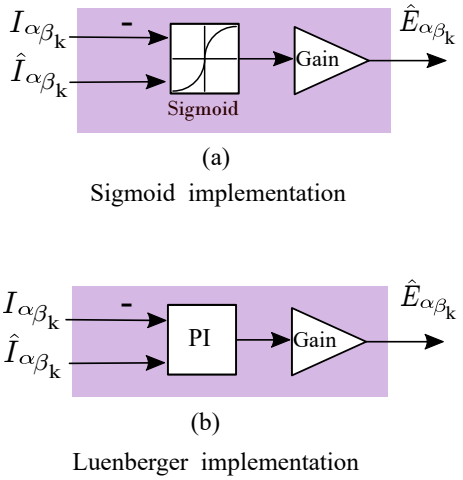

FIGURE 4. The implementation of back EMF estimation loop in case of; a) Sigmoid-based SMO, b) Luenberger Observer.

A. STEADY-STATE PERFORMANCE

Reviewing the behavior of the proposed observer over a range of different speeds is a basic test to determine its steady-state performance. In this test, the performance is examined at 1000 rpm as a rated speed, and 0.2 N.m as a torque load. In addition, the performance is also evaluated through a slow rate of change in speed, where the reference speed profile is ramped from 100 rpm up to 1000 rpm within 8 seconds. Using the I-f startup methodology, Figure 5 shows that the observer loop becomes active after 4.5 seconds, demonstrating the smooth and stable performance of the implicit SMO.

For comparison purpose, Figure 5 shows the speed performance of other two different observer schemes: the sigmoid-based SMO with various tuning values, and the conventional Luenberger observer. The implicit SMO and sigmoid-based SMO at $\lambda = 0.01$ exhibit typical responses with fewer ripples than the other schemes. On the other hand, the Luenberger observer shows more noticeable ripples in the estimated speed, similar to the poorly tuned sigmoid-based SMO with $\lambda = 0.03$. In this test, we can conclude that the implicit SMO offers a steady-state performance comparable to that of a well-tuned sigmoid-based SMO, although the implicit SMO does not in need for parameter adjustment.

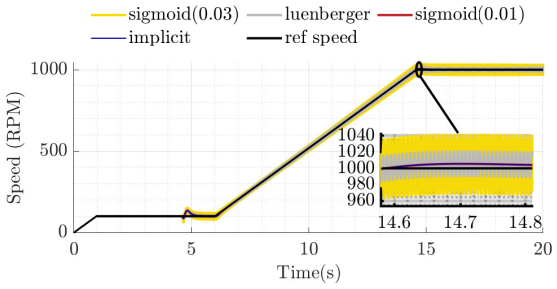

FIGURE 5. Simulation waveform of speed response obtained using: sigmoid-based SMO at $\lambda = 0.01$ (in red), sigmoid-based SMO at $\lambda = 0.03$ (in yellow), luenberger observer (in gray), implicit SMO (in blue).

B. SUDDEN LOAD CHANGE TEST

Here we examine observer's robustness by varying the motor load and monitoring how it remains on target while the load changes. The load suddenly increased from 0.68 N.m to 3.4 N.m at the 15^{th} second. As in the previous test, same profile speed is used here, and also the observer loop becomes active after 4.5 seconds.

Compared to the same observer schemes as in the previous test, Figure 6 shows that the luenberger observer and the sigmoid-based SMO with $\lambda = 0.03$ failed to deal with this sudden change in load. In contrast, the implicit SMO and the sigmoid-based SMO with $\lambda = 0.01$ exhibited robust performance under the same conditions. Both observers effectively managed the sudden load change, quickly adjusting and returning to the reference speed. The similarity in their responses suggests that these observers are well-suited for dynamic scenarios involving rapid load changes, ensuring stability and accuracy in speed estimation.

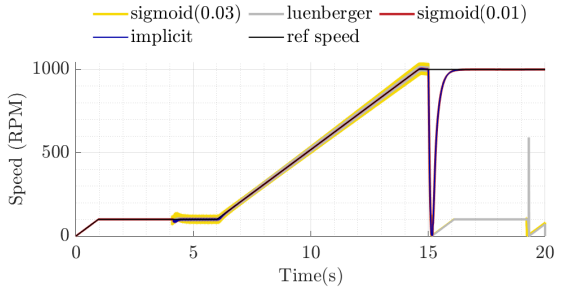

FIGURE 6. Simulation waveform of the estimated speed while a torque load suddenly increased, at the 15^{th} second, from 0.68 N.m to 3.4 N.m.

C. MINIMAL SPEED TEST

The operation of observers at low speed presents several challenges due to a large ratio of the noise component to the estimated signal. The objective of this test is to compare the performance of the proposed observer at low speeds, around 10% to 1.8% of the rated speed. The reference speed was decreased sequentially from 100 rpm to 70 rpm at the 6^{th} second, then down to 50 rpm at the 10^{th} second, and finally reached 18 rpm (1.8% of the rated speed) at the 15^{th} second, all under a load of 0.68 N.m.

Figure 7 illustrates the performance of the examined observers after activating their loops at the second 4.5. Here, the Luenberger observer can no longer maintain operation below 19 rpm. In addition, the Luenberger observer's speed carries higher chatter than the speed estimated by other observer schemes. This performance suggests that the Luenberger observer is not ideal for low-speed scenarios in sensorless SPMSM applications, where accurate estimation is essential. On the other hand, the implicit SMO and sigmoid-based SMO with $\lambda = 0.01$ can maintain stable operation down to 18 rpm. Although these observers are more resilient than the Luenberger observer at low speeds, they are still prone to performance deterioration as the speed approaches the lower limits of the motor's operating range, owing to the inherent characteristics of this region.

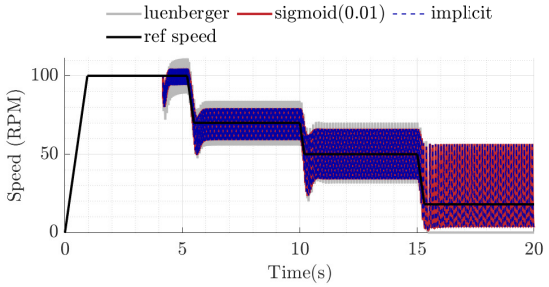

FIGURE 7. Simulation waveform of the estimated speed response during the possible minimum speed obtained using: sigmoid-based SMO with a slope = 0.01, luenberger observer, and implicit SMO.

D. PARAMETER VARIATION PERFORMANCE

Now, we are going to examine the proposed observer against change in motor's parameters. This change may occur when the motor's temperature changes, as a high temperature can duplicate the motor's resistance while reducing the inductance by half. In this test, we maintained the observer settings designed in prior tests based on the motor's nominal values in normal temperature operation. While in motor modeling, we change the motor's resistance and inductance as mentioned above. As well, a load is suddenly increased from 0.32 N.m to 1.6 N.m at the 15^{th} second.

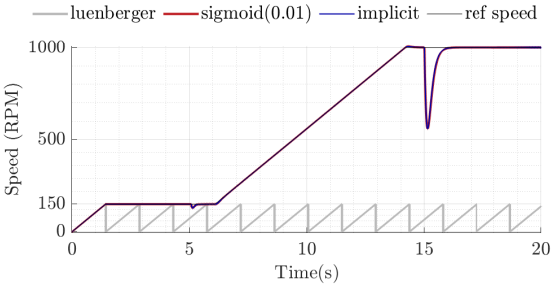

FIGURE 8. Simulation waveform of the estimated speed response while changing the motor resistance and inductance obtained by using: sigmoid-based SMO with a slope = 0.01, luenberger observer, and implicit SMO

Figure 8 shows that the Luenberger observer cannot handle those changes in motor parameters, where it completely failed to produce proper position and speed. In contrast, the nonlinear nature and the robust features of sliding mode systems permit the implicit- and the sigmoid-based SMO to deal with parameter variations and sudden load change. However, the maximum load that the sliding mode-based observers could handle decreased during this test to be around 1.6 N.m. This reduction is expected due to the high level of uncertainty in motor parameters.

V. EXPERIMENTAL VALIDATION

In this section, the proposed observer is applied on experimental setup shown in details in figure 9. The setup consists of a surface permanent magnet synchronous motor (SPMSM), a DC motor as a generator to load the motor, a three-phase inverter and DSP tms320f28379d microcontroller. Two hall-effect sensors are used to sense the motor currents. In order to prove the inverter non-linearities, the tests are carried out under light loads to identify the worst cases.

As outlined in Section IV, we selected the current and speed control as conventional benchmarks to clearly distinguish the effects of the compared observers. Furthermore, we extended the comparison by evaluating the ability of each observer to track specific speed profiles under various operating challenges, including low-speed operation, parameter uncertainties, and different load conditions. Beyond the simulation tests, we introduced a new experiment to highlight the proposed SMO's advantage in reducing computational time.

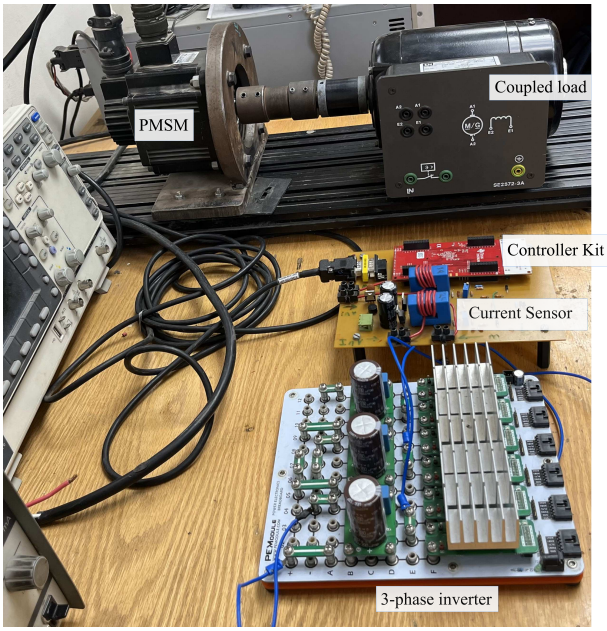

FIGURE 9. Hardware setup

A. DYNAMIC PERFORMANCE

In this section of the experiment, we validate the simulation results that occur in the steady-state test, in which the reference speed profile includes changes in speed levels between 500 rpm down to 70 rpm. The results in Figure 10 show that the Sigmoid-based SMO with $\lambda = 0.03$ causes excessive chattering more than that caused at $\lambda = 0.01$. This emphasizes the importance of carefully selecting and tuning the sigmoid function's rate to prevent performance degradation. the Sigmoid-based SMO with a rate of 0.03 can track the reference speed during the dynamic test, but its performance is notably affected by chattering, especially at higher speeds. On the other hand, the Sigmoid-based SMO with a rate of 0.01, representing a well-tuned observer, shows much better performance with a low level of chattering.

The Luenberger Observer's performance during the speed dynamic test introduces a higher chattering level than that is introduced by the other observers. The Luenberger Observer's linear nature makes it more sensitive to disturbances. The Implicit SMO demonstrates the most robust performance among all the observers tested. The estimated speed closely aligns with the reference speed, exhibiting minimal chattering, much like the well-tuned Sigmoid-based SMO, typically as appeared in simulation results. The implicit method's inherent capability to manage non linearities and disturbances makes it exceptionally effective in maintaining smooth and accurate speed estimation during dynamic transitions.

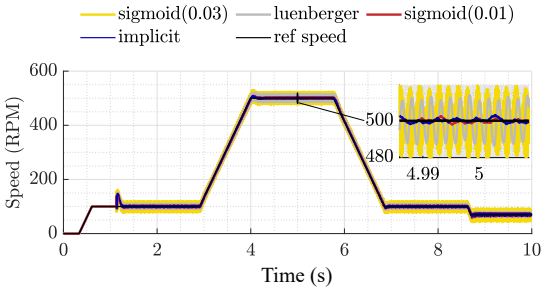

FIGURE 10. Experimental waveform of the estimated speed dynamic response obtained by using: sigmoid-based SMO with different rates 0.01&0.03, luenberger observer, and implicit SMO

B. MINIMAL SPEED TEST

Now, we will confirm the simulation findings of the minimal speed test. The reference speed profile changes from 8% down to 4.2% of the rated speed, where the observers' loop cannot experimentally handle the operation below that range of speed.

The results in Figure 11 indicate that the observers perform differently at low speeds. It was found that the Luenberger Observer had a greater level of ripples in the estimated speed than the other observers and that it was unable to accurately track the speed reference of 42 rpm. The Luenberger Observer was expected to exhibit this behavior since it is a linear estimator, which is more sensitive to non-linearities and disturbances that are more apparent at low speeds. In contrast, the Implicit SMO and the Sigmoid-based SMO with a 0.01 rate showed superior performance, exhibiting lower ripples in the estimated speed. However, it was noted that as the reference speed decreased, the ripples in the speed estimation for these observers increased. This rise in ripples can be attributed to the difficulty of maintaining robust estimation accuracy at very low speeds, where the effects of system non-linearities and noise become more significant.

Among the tested observers, the Implicit SMO demonstrated the best performance during the final test stage, with the reference speed set at 42 rpm. The chattering in the estimated speed was significantly lower compared to the

Sigmoid-based SMO, indicating that the Implicit SMO is more capable of handling the challenges of low-speed operation in sensorless SPMSM control. This is owing to that the implicit SMO is able to reach the intended sliding surface, as stated in Remark 1, unlike the sigmoid-based SMO which requires fine-tuning of its rate to maintain observer performance. This advantage makes the Implicit SMO a more fitting choice for applications where precise speed estimation and control at low speeds are critical.

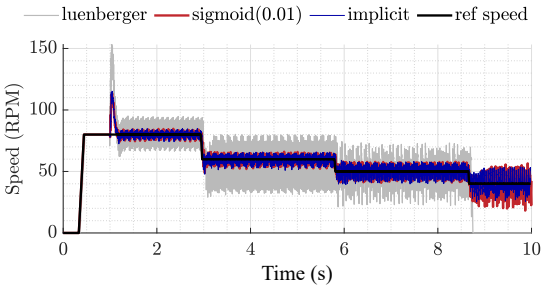

FIGURE 11. Experimental waveform of the estimated speed response during the possible minimum speed obtained by using: sigmoid-based SMO with a slope = 0.01, luenberger observer, implicit SMO

C. PARAMETER VARIATION

Here, we are going to verify the robustness of the proposed observer against parameter variations. As we clarified in the performance evaluation section, we need to examine the observer while the motor's resistance is duplicated and its inductance is reduced by half. To do that experimentally, we designed the observer at the half of motor's resistance and twice of motor's inductance value. As previous tests, the system has to start using I-f start-up method.

As shown in figure 12 (a), the Luenberger observer attained the speed reference (150 rpm) but could not switch from open loop to sensorless mode. Several attempts were made to duplicate the process, but each failed. Similarly, Figure 12(b) depicts the performance of the sigmoid-based SMO with 0.01 rate. The sigmoid-based SMO cannot also shift from open loop to sensorless mode after achieving the speed reference. The process was also repeated several times, but all of them failed. Finally, Figure 12 (c) demonstrates that the implicit SMO handled the parameter variations and successfully transitioned from open loop to sensorless mode, tracing the speed reference correctly with less chattering in the estimated speed.

It should be noticed in Figure 12 (c), although the implicit SMO succeeded to deal with parameter variations, there is still undesired behavior in the starting, where a spike appears around the first sec. of operation. As part of our discussion on this problem, it is noted that the algebraic solution of the implicit Euler discretization requires nominal system parameters, as indicated by the boundaries of the saturation function in (22). While the proposed observer demonstrates robust performance under nominal conditions, significant deviations from these parameters may impact its behavior. Hence, future research may involve developing an efficient method for estimating motor parameters to dynamically update the observer with more accurate parameters, which would enable it to be more adaptable and reliable under diverse operating conditions.

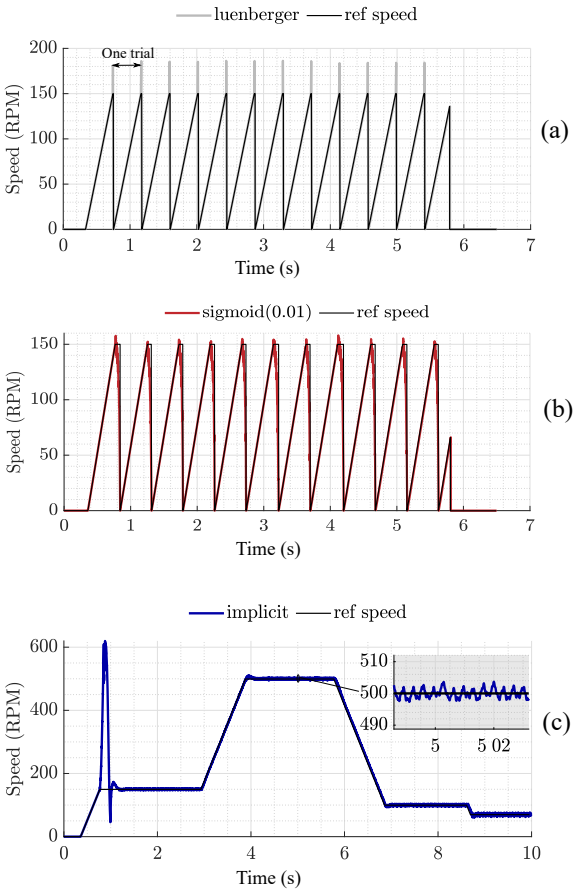

FIGURE 12. Experimental waveform of the estimated speed response while changing the motor resistance and inductance obtained by using: (a)Luenberger Observer (b)Sigmoid-based SMO (0.01 rate) (c)Implicit SMO

D. EXECUTION TIME

When designing and implementing a control algorithm for an embedded system, execution time is an important consideration to ensure the system satisfies its real-time requirements, runs efficiently, and is reliable and stable. Design choices, such as code structure, must be carefully considered to achieve the best possible performance. Figure 13 illustrates the code execution time for the implicit, sigmoid, and Luenberger observers. Based on the results shown, it can be concluded that the implicit and Luneberger observers have the lowest execution time. The total execution time of the implicit SMO is about $21.45\ \mu sec$ and the execution time of the implicit loop itself is about $700\ nsec$. For the Luenberger observer, the total execution time is about $21\ \mu sec$. However, the total execution time of the sigmoid-based SMO is about $24.85\ \mu sec$ and the execution time of the sigmoid function itself is $4.2\ \mu sec$. This shows that the implicit SMO is much faster 5 times than the sigmoid-based SMO.

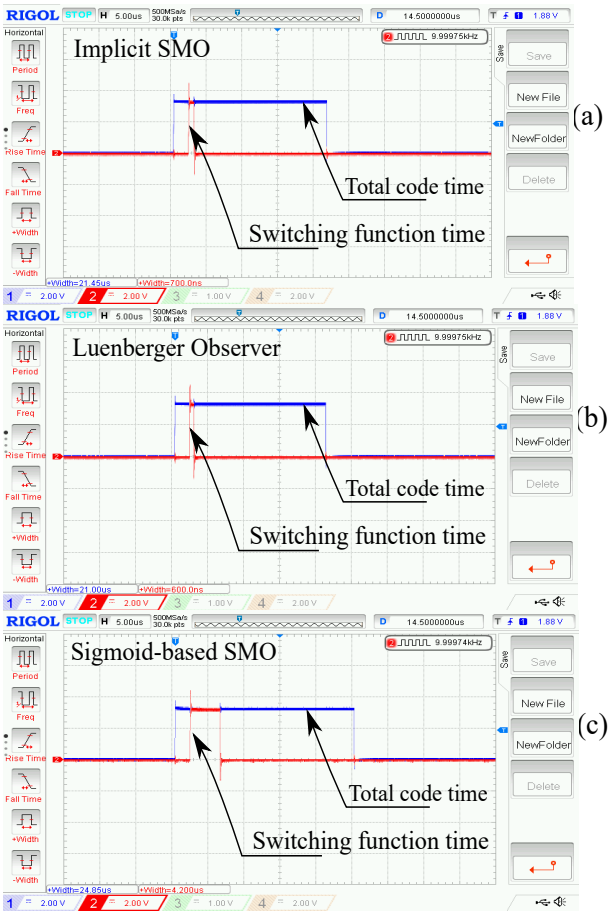

FIGURE 13. Execution time graph with resolution 5μ sec per division. Blue line represents total code time, while red line represents only the execution time of switching function. The sub-graphs show the execution times in case; (a) Implicit SMO, (b)Luenberger Observer, and (c) Sigmoid-based SMO.

VI. CONCLUSION

This paper proposes a novel sliding mode observer for sensorless PMSM motors that aims to simplify design and minimize computational needs while preserving the accuracy and robustness of SMOs. The observer calculates the machine's speed and position using current and voltage measurements based on implicit (backward) Euler discretization, which not only removes chattering but also mimics the behavior of continuous-time sliding mode.

We evaluated the behavior of the proposed observer across a wide range of speeds and torque loads using a simulation approach. The results demonstrated its capability to maintain stability and accuracy under varying conditions when compared to a Luenberger observer and a sigmoid-based Sliding Mode Observer (SMO). Notably, despite the lack of tuning requirements, the implicit SMO exhibited performance comparable to that of a well-tuned sigmoid-based SMO, particularly at steady and nearly steady speeds, as well as during instances of sudden load changes. Furthermore, it displayed superior performance at low speeds relative to other observers. The observer's resilience to variations in motor parameters, specifically resistance and inductance, was also investigated, confirming its adaptability to such changes.

The proposed observer was also implemented and evaluated experimentally, corroborating the findings observed in the simulation results except for the parameter variation test. In this test, the implicit Sliding Mode Observer (SMO) was the only observer scheme capable of adapting to motor uncertainties. Furthermore, we assessed the execution time of each observer in our comparison, revealing that the implicit SMO operates at a faster rate than the sigmoid-based SMO, thereby making it a more efficient option for low-cost embedded systems.

Finally, we can conclude that with the adoption of the implicit technique, the need for additional time-consuming steps to prevent chattering effects is eliminated. Consequently, the simplicity and robustness of the implicit-based SMO make it well-suited for embedded systems where low execution time and operational efficiency are essential as with PMSM control applications.

REFERENCES

[1] O.E. Özçiflikçi, M. Koç, S. Bahçeci, and S. Emiroğlu,"Overview of pmsm control strategies in electric vehicles: a review," *Int. J. Dynam. Control*, 2023.

[2] M. Ezzat, J. de Leon, N. Gonzalez, and A. Glumineau, "Sensorless speed control of permanent magnet synchronous motor by using sliding mode observer," in *2010 11th International Workshop on Variable Structure Systems (VSS)*, pp. 227–232, 2010.

[3] R. Ningning, F. Le, Z. Zan, "Sensorless pmsm control with sliding mode observer based on sigmoid function," *Electr. Eng. Technol.*, vol. 16, pp. 933–939, 2021.

[4] H. Lee and J. Lee, "Design of iterative sliding mode observer for sensorless pmsm control," *IEEE Transactions on Control Systems Technology*, vol. 21, no. 4, pp. 1394–1399, 2013.

[5] S. Ma, J. Zhao, L. Yang, X. Luo, and G. Ran, "Model predictive current control of permanent magnet synchronous motor based on sliding-mode disturbance observer," *IEEJ Transactions on Electrical and Electronic Engineering*, vol. 19,pp. 1068-1078, 2024.

[6] S. Singh and A. Anvari-Moghaddam, "Sensor-based and sensorless vector control of pm synchronous motor drives: A comparative study," in *2018 IEEE 4th Southern Power Electronics Conference (SPEC)*, 2018, pp. 1–6.

[7] Singh Shweta, Tiwari N. Amar, Singh N. Sri, "Speed and Position Estimation for Sensorless Control of PMSM: A Critical Review," *Recent Advances in Electrical & Electronic Engineering* vol. 13, no. 6,pp. 804–822, 2020.

[8] H. Zhang, Z. Yang, L. Fang, and T. Wang, "Research on pmsm control algorithm based on temperature effect," in *2022 9th International Forum on Electrical Engineering and Automation (IFEEA)*, 2022, pp. 1–5.

[9] I. Bakhti, S. Chaouch, A. Makouf, and T. Douadi, "Robust sensorless sliding mode control with luenberger observer design applied to permanent magnet synchronous motor," in *2016 5th International Conference on Systems and Control (ICSC)*, 2016, pp. 204–210.

[10] X. Zhang, G. Tian, Y. Huang, and Z. Lu, "A comparative study of pmsm sensorless control algorithms: Model based vs luenberger observer," in *2016 IEEE Vehicle Power and Propulsion Conference (VPPC)*, 2016, pp. 1–6.

[11] Y. Cao, X. Ren, Q. Guo, G. Wu, Q. Long and M. Ran, "Position Sensorless Control of PMSM Based on EKF Current Noise Compensation and MRAS," *2024 IEEE International Conference on Mechatronics and Automation (ICMA)*, Tianjin, China, 2024, pp. 870-875.

[12] B. Bendjedia and S. Chouireb, "Comparative Study Between Sensorless Vector Control of PMSM Drives based on MRAS, SMO and EKF Observers," *2023 International Conference on Advances in Electronics, Control and Communication Systems (ICAECCS)*, BLIDA, Algeria, 2023, pp. 1-6.

[13] S. K. Spurgeon, "Sliding mode observers: a survey," *International Journal of Systems Science*, vol. 39, no. 8, pp. 751–764, 2008.

[14] A. Messali, M. A. Hamida, M. Ghanes, and M. Koteich, "Robust adaptive sliding mode observer for self-sensing ipmsm control based on optimized hf injection method," *IFAC-PapersOnLine*, vol. 52, no. 16, pp. 556-561, 2019.
[15] Z. Galias and X. Yu, "Complex discretization behaviors of a simple sliding-mode control system," *IEEE Transactions on Circuits and Systems II: Express Briefs*, vol. 53, no. 8, pp. 652–656, 2006.
[16] Z. Galias and X. Yu, "Analysis of zero-order holder discretization of two-dimensional sliding-mode control systems," *IEEE Transactions on Circuits and Systems II: Express Briefs*, vol. 55, no. 12, pp. 1269–1273, Dec 2008.
[17] C. J. V. Filho, D. Xiao, R. P. Vieira, and A. Emadi, "Observers for high-speed sensorless pmsm drives: Design methods, tuning challenges and future trends," *IEEE Access*, vol. 9, pp.56397–56415, 2021.
[18] H. Kim, J. Son, and J. Lee, "A high-speed sliding-mode observer for the sensorless speed control of a pmsm," *IEEE Transactions on Industrial Electronics*, vol. 58, no. 9, pp. 4069–4077, 2011.
[19] W. Xu, A. K. Junejo, Y. Tang, M. Shahab, H. U. Rahman Habib, Y. Liu, and S. Huang, "Composite speed control of pmsm drive system based on finite time sliding mode observer," *IEEE Access*, vol. 9, pp. 151 803–151 813, 2021.
[20] Z. Li, S. Zhou, Y. Xiao and L. Wang, "Sensorless Vector Control of Permanent Magnet Synchronous Linear Motor Based on Self-Adaptive Super-Twisting Sliding Mode Controller," *IEEE Access*, vol. 7, pp. 44998-45011, 2019
[21] D. Liang, J. Li, R. Qu and W. Kong, "Adaptive second-order sliding-mode observer for PMSM sensorless control considering VSI nonlinearity", *IEEE Trans. Power Electron.*, vol. 33, no. 10, pp. 8994-9004, Oct. 2018.
[22] J. R. Domínguez, A. Navarrete, M. A. Meza, A. G. Loukianov and J. Cañedo, "Digital sliding-mode sensorless control for surface-mounted PMSM", *IEEE Trans. Ind. Informat.*, vol. 10, no. 1, pp. 137-151, 2014.
[23] B. Wang, B. Brogliato, V. Acary, A. Boubakir, and F. Plestan, "Experimental comparisons between implicit and explicit implementations of discrete-time sliding mode controllers: Toward input and output chattering suppression," *IEEE Transactions on Control Systems Technology*, vol. 23, no. 5, pp. 2071–2075, 2015.
[24] V. Acary and B. Brogliato, "Implicit euler numerical scheme and chattering-free implementation of sliding mode systems," *Syst. Control Lett.*, vol. 59, no. 5, pp. 284–293, (2010).
[25] O. Huber, V. Acary, and B. Brogliato, "Lyapunov stability analysis of the implicit discrete-time twisting control algorithm," *IEEE Transactions on Automatic Control*, vol. 65, no. 6, pp. 2619–2626, 2020.
[26] X. Xiong, R. Kikuuwe, S. Kamal, and S. Jin, "Implicit-euler implementation of super-twisting observer and twisting controller for second-order systems,"*IEEE Transactions on Circuits and Systems II: Express Briefs*, vol. 67, no. 11, pp. 2607–2611, 2020.
[27] R. Hermann and A. Krener, "Nonlinear controllability and observability,"*IEEE Transactions on Automatic Control*, vol. 22, no. 5, pp. 728–740, October 1977.
[28] M. G. D. Zaltni, M. N. Abdelkrim and J. P. Barbo, "Observability analysis of pmsm," in *2009 3rd International Conference on Signals, Circuits and Systems (SCS)*, 2009, pp. 1–6.
[29] P. Vaclavek, P. Blaha, and I. Herman, "Ac drive observability analysis," *IEEE Transactions on Industrial Electronics*, vol. 60, no. 8, pp. 3047–3059, 2013.
[30] R. Kikuuwe, S. Yasukouchi, H. Fujimoto, and M. Yamamoto, "Proxy-based sliding mode control: A safer extension of PID position control," *IEEE Trans. Robot.*, vol. 26, no. 4, pp. 670–683, 2010.
[31] O. Huber, V. Acary, and B. Brogliato, "Lyapunov stability and performance analysis of the implicit discrete sliding mode control," *IEEE Transactions on Automatic Control*, vol. 61, no. 10, pp. 3016–3030, 2016.
[32] M. S. El-Daleel, O. Mahgoub, A. L. Elshafie, and A. Mahgoub, "Dead-time compensation via adaptive lookup table reconstruction for low-speed operation," in *2020 IEEE International Conference on Power Electronics, Drives and Energy Systems (PEDES)*. IEEE, 2020, pp. 1–6.
[33] Z. Wang, K. Lu, and F. Blaabjerg, "A simple startup strategy based on current regulation for back-emf-based sensorless control of pmsm," *IEEE Transactions on Power Electronics*, vol. 27, no. 8, pp. 3817–3825, 2012.
[34] J. Xing, Z. Qin, C. Lin, and X. Jiang, "Research on startup process for sensorless control of pmsms based on i-f method combined with an adaptive compensator," *IEEE Access*, vol. 8, pp. 70 812–70 821, 2020.

NEHAL BAIOMY received her B.S. and M.S. degrees in Electrical Engineering from Cairo University, Egypt in 2011 and 2014, respectively, and her Ph.D. degree from Kyushu University, Fukuoka, Japan, in 2020. She is currently an assistant professor at Cairo University, Egypt. Her research interests include sliding mode control, adaptive control, linear matrix inequality (LMI), wind turbine control, and drives control.

MOHAMED MAHMOUD ABDELHAFIZ received the bachelor's degree in electrical power engineering from Cairo University, in 2018, where he is currently pursuing the master's degree. He is also maintenance engineer at GASCO. His research interests include Control of power electronics, Sliding mode observers, machine drives.

ABDELMOMEN MAHGOUB received the B.Sc. and M.Sc. degrees. in electrical power engineering from Cairo University, Giza, Egypt, in 2008 and 2010, respectively, and the Ph.D. degree in electrical engineering from the Kyushu University, Kyushu, Japan, in 2014. He was a Post-Doctoral Fellow with Università degli Studi del Sannio, Italy. He is currently an associate professor, Cairo University, Egypt. His current research interests include the control of power electronic converters, machine drives, resonant converters, multilevel inverters, and renewable energy systems.